International Journal of Nanoscience, Vol. 1, No. 1 (2002) 41–51

NANOBELTS OF SEMICONDUCTIVE OXIDES: A STRUCTURALLY AND MORPHOLOGICALLY CONTROLLED NANOMATERIALS SYSTEM

ZHONG LIN WANG* and ZHENGWEI PAN

Center for Nanoscience and Nanotechnology
School of Materials Science and Engineering
Georgia Institute of Technology, Atlanta, GA 30332-0245, USA
**zhong.wang@mse.gatech.edu*

Received 29 October 2001

We have developed a simple and economic technique for synthesis of one-dimensional nanobelt structures of semiconductive oxides such as ZnO, SnO_2, In_2O_3, CdO, Ga_2O_3 and PbO_2. The as-synthesized oxide nanobelts are pure, structurally uniform, single crystalline and most of them free from dislocations; they have a rectangular-like cross-section with typical widths of 30–300 nanometers, width-to-thickness ratios of 5–10 and lengths of up to a few millimeters. The belt-like morphology appears to be a unique and common structural characteristic for the family of semiconducting oxides with cations of different valence states and materials of distinct crystallographic structures. The nanobelts are structurally and morphologically controlled and they are intrinsic semiconductors, providing a new system after carbon nanotubes for a systematic understanding on dimensionally confined transport phenomena in functional oxides. They are also ideal building blocks for fabrication of nanoscale devices based on the integrity of individual nanobelts.

Keywords: Nanobelts; ZnO; SnO_2; CdO; nanosheets.

1. Introduction

As feature sizes approaching submicron scale, one of the major challenges to the next generation microelectronics is interconnect that link and transmit information across the devices. One-dimensional structures have attracted a great deal of attention due to their unique properties and potential for future technology. Much of the studies of one-dimensional like structures have been focused on carbon nanotubes,[1] have been extensively studied in the last decade. Recently, silicon nanowires[2,3] and compound semiconductor nanowires,[4] such as InP have attracted a great deal of attention because they can be used as the fundamental building blocks for nanoelectronics.

It has been demonstrated in laboratory and in industry that wide bandgap binary semiconducting oxides, such as ZnO, SnO_2, In_2O_3 and CdO, are transparent

conducting oxide (TCO) materials[5] that can be used for sensors,[6] surface coating, smart windows and electro-optical materials due to their various unique properties. For example, fluorine-doped SnO_2 film is widely used in architectural glass applications because of its low emissivity for thermal infrared heat,[5] SnO_2 nanoparticles are regarded as one of the most important sensor materials for detecting leakage of several inflammable gases owing to its high sensitivity to low gas concentrations;[5] tin-doped indium oxide (In_2O_3:Sn, ITO) film is an ideal material for flat panel displays (FPDs) due to its high electrical conductivity and high optical transparency;[5] ZnO is regarded as an ideal alternative material for ITO in some future display applications because of its lower cost and easier etchability.[5]

Recently, our research has taken a slightly different approach with an emphasis on functional oxides, which are believed to be the most important smart materials for future technology. Some of the transition and rare earth metal oxides are semiconductive and they are the fundamental to the development of the smart and function devices, which have key applications in electro-mechanical, electro-optical, electro-chemical and opto-thermal applications. The metal oxides will have two important characteristics including (1) cations with mixed valences and (2) significant oxygen vacancies. The oxides are usually made into single crystals, dispersive nanoparticles, or condensed films. Their properties are tailored and tuned by adjusting oxygen deficiency and cation valences. This paper reviews our most recent advances in the synthesis and characterization of semiconductive oxide nanowires and nanobelts. Some of the future prospects of the nanobelts are presented.

2. Experimental Method

Our synthesis is based on thermal evaporation of oxide powders under controlled conditions without the presence of catalyst.[7] The desired oxide powders were placed at the center of an alumina tube that was inserted in a horizontal tube furnace (Fig. 1), where the temperature, pressure and evaporation time were controlled. At one end of the furnace, argon or nitrogen flows over a crucible containing the raw powder of interest. The total tube pressure in the inner tube can be made to range from 200 to 650 Torr. This pressure is controlled by a mechanical pump attached to the inner alumina tube through the downstream stainless steel end piece. This end piece is mechanically attached to a "water cooled" cold plate. In our experiments, except for the evaporation temperature that was determined based on the melting point of the oxides to be used, we kept following parameters to be constant: evaporation time, two hours; chamber pressure, 300 Torr; and Ar flowing rate, 50 standard cubic centimeter per minute (sccm). During evaporation, the products were deposited onto an alumina plate placed at the downstream end of the alumina tube.

The as-deposited products were characterized and analyzed by X-ray diffraction (XRD) (Philips PW 1800 with Cu Kα radiation), scanning electron microscopy (SEM) (Hitachi S800 FEG), transmission electron microscopy (TEM) (Hitachi

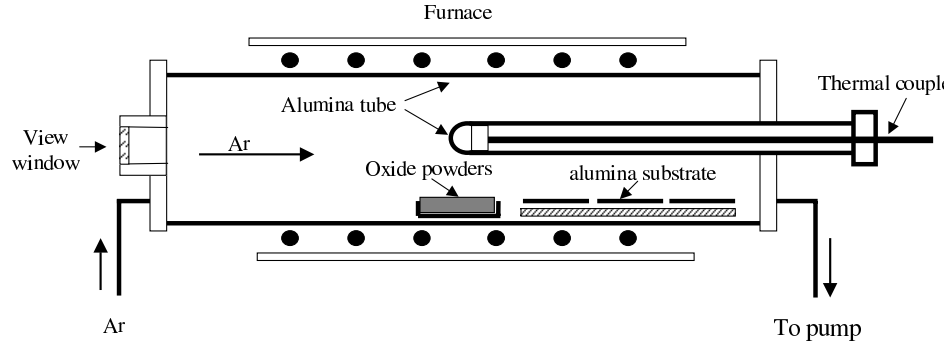

Fig. 1. Experimental set up for the synthesis of nanobelt structures.

HF-2000 FEG at 200 kV and JEOL 4000EX high resolution TEM (HRTEM) at 400 kV), and energy dispersive x-ray spectroscopy (EDS).

3. Experimental Results

3.1. *Nanobelts*

The current studies of semiconducting oxides have been focused on two-dimensional (2D) films and zero-dimensional (0D) nanoparticles, which can be readily synthesized using various well-established techniques such as sputtering (for films) and sol-gel (for particles). Nanostructured oxides of functional materials, such as SnO_{2-x}, and TiO_2, have important applications in sensors and fuel cells. It is well known that nanostructured SnO_{2-x} is a material that can be used to detect gases such as CO and H_2 at the level of a few hundreds of ppm. Not only are the unique structures of the SnO_{2-x} nanowires, which we are beginning to synthesize likely to be important in the study of one-dimensional ionic and electric transport properties of the metal oxides but also these nanowires appear ideally suited for fabricating nanosize sensors with large surface area. Further, with a judicious choice of metallic tin in the Sn/SnO mixtures, it should be possible to create intermediate SnO_{2-x} structures.

By thermal evaporation of ZnO powders (purity: 99.99%, melting point: 1975°C) at 1400°C for two hours, white wool-like products were formed in a high yield on the surface of the alumina plate. SEM observations reveal that the products consist of a large quantity of 1D nanostructures with typical lengths in the range of several tens to several hundreds of micrometers; some of them even have lengths on the order of millimeters (Fig. 2). EDS microanalysis and powder XRD measurement show that the sample is wurtzite (hexagonal) structured ZnO. Through TEM images, we found that the geometrical shape of the ZnO 1D nanostructures is a belt that is distinct in cross-section from the previously reported nanotubes[1] and nanowires.[2–4] Each nanobelt has a uniform width along its entire length, and the typical widths of the nanobelts are in the range of 50–300 nm.[7] No particle was observed at the ends of the nanobelts. A ripple-like contrast observed in TEM image is due to strain

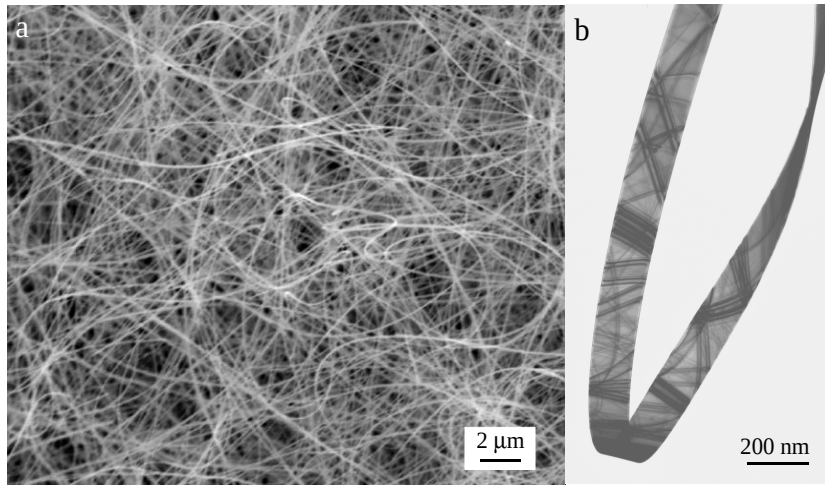

Fig. 2. Ultra-long nanobelt structure of ZnO (a) SEM image of the as-synthesized ZnO nanobelts with high purity and crystallinity. (b) Bright-field TEM image showing the bent belt shape. The contrast observed in TEM image is due to bending strain.

resulted from the bending of the belt. The typical thickness and width-to-thickness ratios of the ZnO nanobelts are in the range of 10–30 nm and ∼5–10, respectively, as determined from several tens of nanobelts. HRTEM and electron diffraction show that the ZnO nanobelts are structurally uniform and single crystalline but with two different growth directions. The nanobelt, growing along [0001] and enclosed by $(2\bar{1}\bar{1}0)$ and $(01\bar{1}0)$ facets, shows no defect and no dislocation; the one, growing along $[01\bar{1}0]$ and enclosed by (0001) and $(2\bar{1}\bar{1}0)$ facets, is also dislocation free but with only a single stacking fault that is parallel to the axis and runs throughout the entire length of the nanobelt. The surfaces of the nanobelts are clean, atomically sharp and without any sheathed amorphous phase.

Single crystalline SnO_2 nanobelts of rutile structure can consistently be synthesized by thermal evaporation of either SnO_2 powders (purity: 99.9%, melting point: 1630°C) at 1350°C or SnO powders (purity: 99.9%, melting point: 1080°C) at 1000°C.[8] After evaporation, similar white fuzz-like products were deposited on the alumina plate, regardless the source material was SnO_2 or SnO. SEM imaging (Fig. 3(a)) and EDS analysis show that the products are composed of a large quantities of ultra-long SnO_2 nanobelts (with lengths up to the order of millimeters) and a small fraction of Sn nanoparticles (as indicated by arrowheads in Fig. 3(a)). XRD patterns from the as-synthesized nanobelt samples prove the rutile type structure with lattice constants of $a = 4.722$ Å and $c = 3.184$ Å, which are consistent with those of bulk SnO_2. TEM images shown in Fig. 3(b) clearly display the shape characteristic of the SnO_2 nanobelts. Analogy to the case of ZnO nanobelts, the ripple-like strain contrast can also be seen in SnO_2 nanobelts. Each nanobelt is uniform in width and thickness, and the typical widths of the SnO_2 nanobelts are

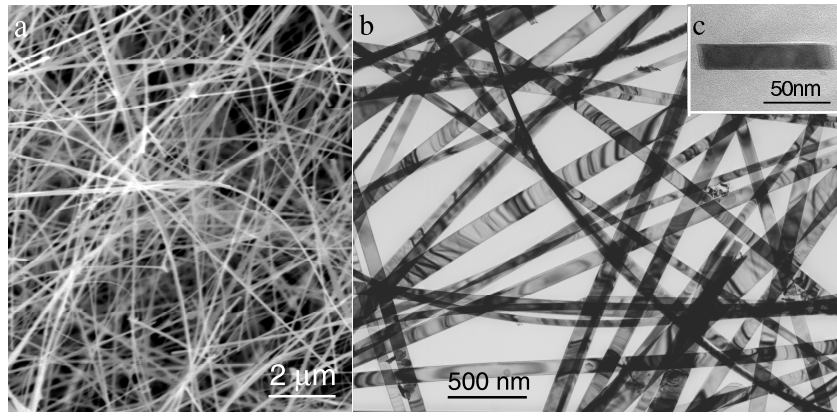

Fig. 3. (a) SEM image of the as-synthesized SnO_2 nanobelts. (b) Low magnification bright-field TEM image showing the crystalline structure of the nanobelts. (c) A cross-sectional TEM image of a nanobelt.

in the range of 50–200 nm. Cross-sectional TEM observations show that the cross-sections of the SnO_2 nanobelts are rectangular-like, with typical width-to-thickness ratios of $\sim$ 5–10. High-resolution TEM image reveals that the nanobelts are single crystalline and dislocation free. Electron diffraction pattern indicates that the SnO_2 nanobelt grows along [101], and it is enclosed by (010) and $(10\bar{1})$ crystallographic facets.

Nanoribbons and flat nanosheets of Ga_2O_3 have also been synthesized by our technique.[9] The as-synthesized nanoribbons and nanosheets are pure, structurally uniform, single crystalline and free from dislocations. The nanoribbons and the nanosheets all have monoclinic β-Ga_2O_3 structure. The flat top and bottom surfaces for both nanoribbons and nanosheets are $\pm(100)$, the side surfaces are $\pm(010)$ and $\pm(10\bar{1})$ for nanoribbons and $\pm(010)$, $\pm(10\bar{1})$ and $\pm(21\bar{2})$ for nanosheets. The axis direction of nanoribbon growth is along either [001] or [010].

β-PbO_2 nanobelts, with a rectangular cross-section, a typical length of 10–200 μm, a width of 50 to 300 nm and a width-to-thickness ratio of 5 to 10, have also been successfully synthesized by elevated evaporation of commercial PbO powders at high temperature.[10] Different from the growth of nanobelts of other oxides, each PbO_2 nanobelt is found to have a large polyhedral Pb tip at one of its ends, suggesting the growth is dominated by a vapor–liquid–solid mechanism. Electron beam irradiation of the PbO_2 nanobelts results in the phase transformation from PbO_2 to PbO and finally to Pb.

Using a mixture of Sn and SnO_2, an new type of SnO_{2-x} nanoribbons has been synthesized. In addition to the normal rutile structured SnO_2, it has been possible to form an orthorhombic superlattice-like structure. The orthorhombic structure usually can only exist at 150 kbar for bulk materials, but it presents in the nanoribbons at one atomosphere, which is a distinct feature of the nanostructure.[11]

Table 1. Semiconductive oxide nanobelts and their growth directions and surface planes. *The nanobelts have a single stacking fault/twin parallel to the growth direction throughout the entire length.

Nanobelts	Crystal structure	Growth direction/Plane	Top surface	Side surfaces
ZnO	Wurtzite	[0001]	$\pm(2\bar{1}\bar{1}0)$	$\pm(01\bar{1}0)$
ZnO	Wurtzite	$[01\bar{1}0]$*	$\pm(2\bar{1}\bar{1}0)$	$\pm(0001)$
Ga_2O_3	Monoclinic	[001]	$\pm(100)$	$\pm(010)$
Ga_2O_3	Monoclinic	[010]	$\pm(100)$	$\pm(10\bar{1})$
SnO_2	Rutile	[101]	$\pm(10\bar{1})$	$\pm(010)$
In_2O_3	C-Rare earth	[001]	$\pm(100)$	$\pm(010)$
CdO	NaCl	[001]	$\pm(100)$	$\pm(010)$
PbO_2	Rutile	[010]	$\pm(201)$	$\pm(10\bar{1})$

Our results show that the belt-like morphology is a common and unique structural characteristic for some semiconducting oxides with cations of different valence states and materials of different crystallographic structures. This is a distinctly different structure from the reported semiconductor nanowires. The belt-like morphology appears to be a unique and common structural characteristic for the family of semiconductive oxides with cations of different valence states and materials of distinct crystallographic structures.[7,8] Their structures are well controlled, and the belt shape is defined by some specific crystallographic planes. Table 1 gives a summary on the growth directions and the surface planes of the nanobelts of different materials that we have successfully synthesized. The semiconductive oxide nanobelts could be used for fabrication of nanoscale electronic and optoelectronic devices. With a well-defined geometry and perfect crystal structure, the nanobelts are likely to be a model materials family for a systematic understanding in the electrical, thermal, optical and ionic transport processes as well as mechanical behavior in quasi-one-dimensional nanostructures with the absence of dislocations. This will be an exciting new field for nanomaterials.

3.2. *Nanosheets*

CdO has a NaCl-type crystals structure, and its (100), (010) and (001) surfaces are identical. Therefore, the growth can be either along [100], [010] or [001], thus, it is possible to have different growth morphologies. If we only have two possible choices for growth directions such as [100] and [010], we can have the platelet structures as displayed in Fig. 4, where most of the facets are (100) and (010), while the (110) type of faces is also seen, which is introduced to minimize the surface area possibly for reducing the total surface energy. These structures have a common character that the surface normal is [001], displaying sheet-type of structure. The various shapes shown in Fig. 4 are induced by the {100} and {110} type of facets. These sheets are single crystalline and they have no dislocations and no planar defects.

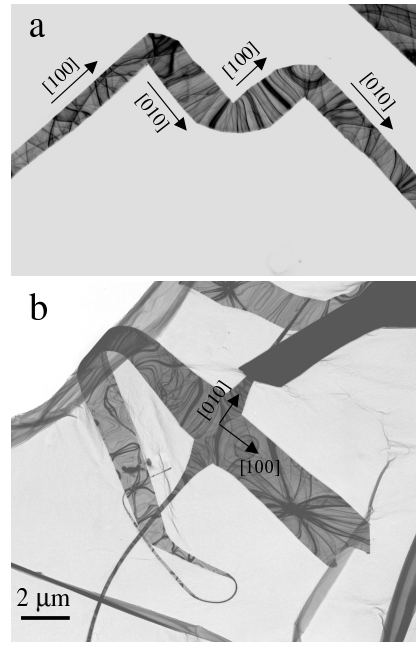

Fig. 4. TEM images of CdO nanobelts and nanosheets, showing their growth along [100] and [010].

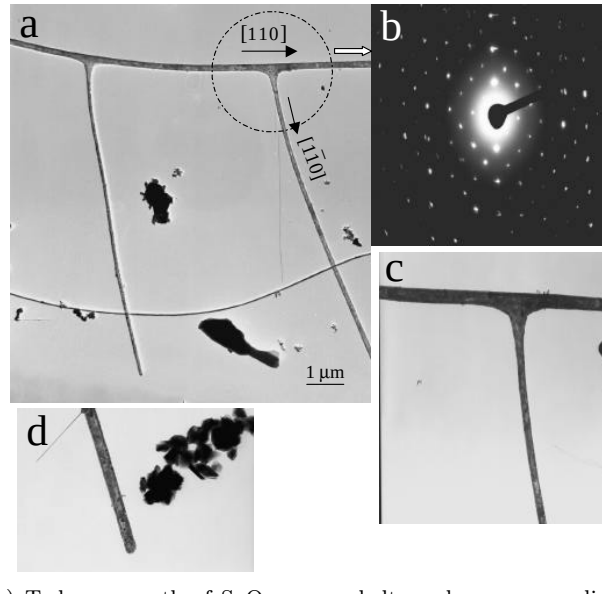

Figs. 5(a) and (b) T-shape growth of SnO_{2-x} nanobelts and a corresponding electron diffraction pattern from the T-region, showing the T-shape structure is single crystalline. (c) and (d) Magnified images from the T-region and the tip of an arm.

It is interesting to point out that, although the growth along [100], [010] and [001] are equivalent, no cube was found in our growth product.

3.3. *Growth kinetics in controlling the nanowire morphology*

The morphology of the nanobelts is defined by a combination of surface energy and growth kinetics. The low-energy surfaces defines the planes that can present in the final growth product, while the growth kinetics determines the surface ratios among different planes. Figure 5 shows another example of the growth of the single crystalline T-shape SnO_{2-x} nanowire. The electron beam direction is [101]; the straight nanowire grows parallel to the $(1\bar{2}\bar{1})$ plane, then the growth direction switches to be parallel to the $(12\bar{1})$ plane. The T-shape was resulted from the growth parallel to $(1\bar{2}\bar{1})$ and $(12\bar{1})$, which are two crystallographically equivalent planes. Electron diffraction pattern recorded from the T-junction shows its single crystalline structure (Figs. 5(b) and 5(c)). Images recorded from the growth front of the T branch shows the absence of catalytic particle, indicating that the formation of the T shape is not the result of catalytically guided growth (Fig. 5(d)). It is apparent that the growth morphology is largely determined by growth kinetics.

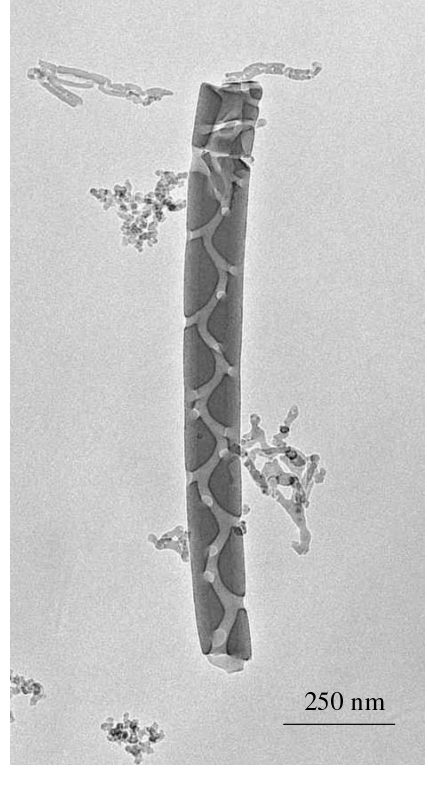

Fig. 6. TEM image of an unusual silica nanowire.

Another very interesting morphology we observed was for SiO_2 nanowires. Shown in Fig. 6 is a segment of a silica nanowire synthesized by a technique similar to that we used for the synthesis of nanobelts. The nanowire has an inner channel that screw-up along the axis of the wire and penetrates the surface whenever it reaches the nearest surface point. The nanowire is amorphous and the formation of the channel is believed to have nothing to do with surface energy, instead, such a configuration cannot be the lowest energy configuration of the nanowire. The channel is formed possibly due to the variation in growth conditions such as temperature fluctuation, gas flow, etc.

4. Discussion and Conclusion

We have demonstrated that a control of growth conditions can produce a variety of unique semiconductor based nanobelts. The nanobelts have a controlled morphology, and their surfaces are defined by specific crystallographic planes. The volume of the nanobelts is free from dislocations, although a single planar defect (twin or stacking fault) may present parallel to the growth direction. These belts are ideal model systems for a systematic understanding of electrical, thermal, and optical transport processes in dislocation-free nanowires.

In contrast, the structures of carbon nanotubes are rather difficult to control, especially the helical angles. It is known that the metallic or semiconductive nature of carbon nanotubes is determined by the helical angle, which is a key quantity in the electronic applications of carbon nanotubes. This may be a main hurdle in the application of carbon nanotubes for electronic and optoeletronic devices. The functional oxides presented here are mostly wide-gap semiconductors. The bandgap is ~ 3.2 eV for ZnO, ~ 3.65 eV for SnO_2, and 3.7 eV for In_2O_3. These materials are ideal candidates for optoelectronics. The nanobelt structures of these oxides are semiconductors, which are predetermined by the intrinsic structure of the oxides. The finite size of the nanobelts in the thickness and possibly width directions may provide a parameter for tuning their electronic structure. In fact, the thin films of these oxides have profound applications in industry for a variety of purposes, and by doping, their properties can be dramatically improved and tuned (Tables 2 and 3).

The semiconducting oxide nanobelts could be doped with different elements and be used for fabricating nanosize sensors based on the characteristics of individual nanobelts. The nanobelts could also be used for fabrication of nanoscale electronic

Table 2. Resistivity ($\mu\Omega$ cm) of dopped oxides in comparison to Ag (from Ref. 13).

Ag	1.6
In_2O_3:Sn	100
ZnO:Al	150
SnO_2:F	200

Table 3. Tuning the properties by dopping (from Ref. 13).

Highest transparency	ZnO:F
Highest conductivity	In_2O_3:Sn
Lowest plasmon frequency	ZnO:F, SnO_2:F
Highest plasmon frequency	In_2O_3:Sn
Highest work function	SnO_2:F
Lowest work function	ZnO:F
Best thermal stability	SnO_2:F
Best mechanical stability	SnO_2:F
Best chemical stability	SnO_2:F
Easiest to etch	ZnO:F
Best resistance to H plasmons	ZnO:F
Least toxic	ZnO:F, SnO_2:F
Lowest cost	SnO_2:F

and optoelectronic devices because they are semiconductors. Other possible applications can be in flat panel display and smart windows. It has been demonstrated that nanoscale diode can be fabricated using the cross-junction of two InP semiconductor nanowires.[12] Nanowires of ZnO have been shown to give lasers,[13] promising their applications in nanoscale optoelectronic devices. With a well-defined geometry and perfect crystal structure, the semiconducting oxide nanobelts have achieved structural control. They are likely to be a model materials family for understanding the electrical, thermal, optical and ionic transport processes in quasi-one-dimensional nanostructures.

The integrity of individual nanobelts is mostly suitable for building nanosize gas and chemical sensors. A successful effort will greatly impact the miniaturization of sensors and improve their sensitivity. If successful, it may lead to major technological breakthroughs in the field of nanosize sensors for low power consumption and high sensitivity. Such devices may have unique applications in biology and the biomedical sciences for early diagnostics and in-situ monitoring.

Acknowledgment

Thanks for the support from NSF grants DMR-9733160.

References

1. S. Iijima, *Nature* **354**, 56 (1991).
2. S. T. Lee, N. Wang, Y. F. Zhang, and Y. H. Tang, *MRS Bulletin* **36** (August 1999).
3. D. P. Yu, Z. G. Bai, Y. Ding, Q. L. Hang, H. Z. Zhang, J. J. Wang, Y. H. Zou, W. Qian, G. C. Xiong, H. T. Zhou, and S. Q. Feng, *Appl. Phys. Lett.* **72**, 3458 (1998).
4. A. M. Morales and C. M. Lieber, *Science* **279**, 208 (1998).
5. D. S. Ginley and C. Bright (eds.), *Mater. Res. Soc. Bull.* **25**, 15 (2000); and all the articles in this special issue.

6. N. Yamazoe, *Sensors and Actuators B* **5**, 7 (1991).
7. Z. W. Pan, Z. R. Dai, and Z. L. Wang, *Science* **291**, 1947 (2001).
8. Z. R. Dai, Z. W. Pan, and Z. L. Wang, *Solid State Comm.* **118**, 351 (2001).
9. Z. R. Dai, Z. W. Pan, and Z. L. Wang, *J. Phys. Chem. B* **106**, 902 (2002).
10. Z. W. Pan, Z. R. Dai, and Z. L. Wang, *Appl. Phys. Lett.* **80**, 309 (2002).
11. Z. R. Dai, J. L. Gole, J. D. Stout, and Z. L. Wang, *J. Phys. Chem. B* **106**, 1274 (2002).
12. X. F. Duan, Y. Huang, Y. Cui, J. Wang, and C. M. Lieber, *Nature* **409**, 66 (2001).
13. M. H. Huang, S. Mao, H. Feick, H. Q. Yan, Y. Y. Wu, H. Kind, E. Weber, R. Russo, and P. D. Yang, *Science* **292**, 1897 (2001).
14. R. G. Gordon, *MRS Bulletin* **52** (August 2000).